Anisotropic dependence of the magnetic transition on uniaxial pressure in the Kondo semiconductors CeT_2Al_{10} (T = Ru and Os)

K. Hayashi,[1] K. Umeo,[2] T. Takeuchi,[1] J. Kawabata,[1] Y. Muro,[3] and T. Takabatake[1,*]

[1]*Graduate School of Advanced Sciences of Matter, Hiroshima University, Higashi-Hiroshima 739-8530, Japan*

[2]*Cryogenic and Instrumental Analysis Division, N-BARD, Hiroshima University, Higashi-Hiroshima 739-8526, Japan*

[3]*Liberal Arts and Sciences, Faculty of Engineering, Toyama Prefectural University, Imizu 939-0398, Japan*

(Received 29 September 2017; revised manuscript received 3 December 2017; published 21 December 2017)

We have measured the strain, magnetization, and specific heat of the antiferromagnetic (AFM) Kondo semiconductors CeT_2Al_{10} (T = Ru and Os) under uniaxial pressures applied along the orthorhombic axes. We found a linear dependence of T_N on the b-axis parameter for both compounds under uniaxial pressure $P \parallel b$ and hydrostatic pressure. This relation indicates that the distance between the Ce-T layers along the b axis is the key structural parameter determining T_N. Furthermore, the pressure dependence of the spin-flop transition field indicates that Ce-Ce interchain interactions stabilize the AFM state with the ordered moments pointing to the c axis.

DOI: 10.1103/PhysRevB.96.245130

I. INTRODUCTION

Most cerium-based compounds have metallic ground states in which the effective mass of quasiparticles is largely enhanced by the hybridization of localized $4f$ electrons with conduction electrons, known as c-f hybridization [1]. In a few Ce-based compounds, however, the c-f hybridization gives rise to a narrow gap at the Fermi level E_F, leading to a semiconducting ground state [2]. For example, an orthorhombic compound CeNiSn [3], a cubic one $Ce_3Bi_4Pt_3$ [4], and a tetragonal one $CeRu_4Sn_6$ [5] possess an energy gap at low temperatures, and thus are called Kondo semiconductors (KSs). The ground state of all KSs is nonmagnetic because the $4f$ moments of Ce ions are fully compensated by the conduction electrons. Recently, orthorhombic compounds CeT_2Al_{10} (T = Ru and Os) with the $YbFe_2Al_{10}$-type structure have been found to show semiconducting transport properties and yet exhibit an antiferromagnetic (AFM) transition at around 28 K [6–9]. Further, the magnetic moments of $0.3-0.4\,\mu_B$/Ce are alternatingly oriented along the c axis, forming a zigzag chain as shown in Fig. 1(a) [10,11]. In view from the c direction, the chains arrange in a rhombus with an angle θ of 83 deg, as shown in Fig. 1(b).

The AFM order has two unusual characteristics. One is the unexpectedly high-ordering temperatures T_N, i.e., 27 and 28.5 K for T = Ru and Os, respectively, which are higher by 10 K than T_N of the Gd counterparts [12,13]. A promising model for the AFM order at high T_N was proposed by a study of polarized optical conductivity for $CeOs_2Al_{10}$ [14]. The study has revealed that a kind of charge density wave (CDW) develops along the b axis at 36 K far above T_N. The crystal structure presented in Fig. 1(a) can be viewed as constructed from Ce-T layers stacking along the b axis. Then, it was proposed that opening of the CDW-like gap along the b axis induces the AFM order [14]. The other strange fact is that the direction of ordered moments μ_{AFM} along the c axis is different from the a axis that is the easy magnetization axis preferred by the crystal field effect in the paramagnetic state [15,16]. To explain this puzzle, it was conjectured that the strong hybridization along the a axis prevents the moments from pointing to the a axis [17]. Despite extensive studies, the relation among the anisotropic c-f hybridization, AFM transition at high T_N, and ordered moment direction along the hard axis remains unresolved.

Let us briefly summarize the structural and magnetic properties. In the series of compounds LnT_2Al_{10} (Ln: lanthanides), the orthorhombic lattice parameters decrease on going from Ln = La to Ln = Lu according to the lanthanide contraction [13,17]. The anisotropic contraction for Ln = Ce suggested that the c-f hybridization in the a-c plane is stronger than along the b direction. An x-ray photoemission spectroscopic study showed that the effective c-f hybridization in T = Os is larger by 7.5% than in T = Ru [18]. It is known that stronger hybridization leads to higher Kondo temperature T_K. The value of T_K was estimated using the relation $T_K = 3T_{\chi m}$, where $T_{\chi m}$ is the temperature at the maximum of the magnetic susceptibility [2]. Then, T_K of 135 K for T = Os is higher than that of 90 K for T = Ru [7,8].

Application of hydrostatic pressure on Ce compounds strengthens the c-f hybridization, leading to delocalization of the $4f$ electron state [19]. For $CeRu_2Al_{10}$ under pressures, the temperature dependences of both resistivity and magnetic susceptibility approximate those of $CeOs_2Al_{10}$ under ambient pressure [7,20,21]. This fact is consistent with the stronger c-f hybridization in T = Os than in T = Ru, as mentioned above. For T = Ru and Os, T_N increase to the maxima at 32 and 29 K, and abruptly disappear at 4.8 and 2.5 GPa, respectively [7,21]. This dependence of T_N seems to be consistent with a recent phase diagram of T_N as a function of the Kondo exchange coupling, which has been constructed by the dynamical mean-field calculation for an anisotropic Kondo lattice model [22].

Concerning the AFM structure of CeT_2Al_{10}, it is noteworthy that the direction of μ_{AFM} is easily changed by applications of magnetic field and pressure as well as atomic substitution [23–26]. The magnetic field applied along the c axis induces a spin-flop transition from $\mu_{AFM} \parallel c$ to $\mu_{AFM} \parallel b$ at $B^* = 4$ and 7 T for T = Ru and Os, respectively [23,8]. The reorientation, not along the easy a axis but along the hard b axis, was

*Corresponding author: takaba@hiroshima-u.ac.jp

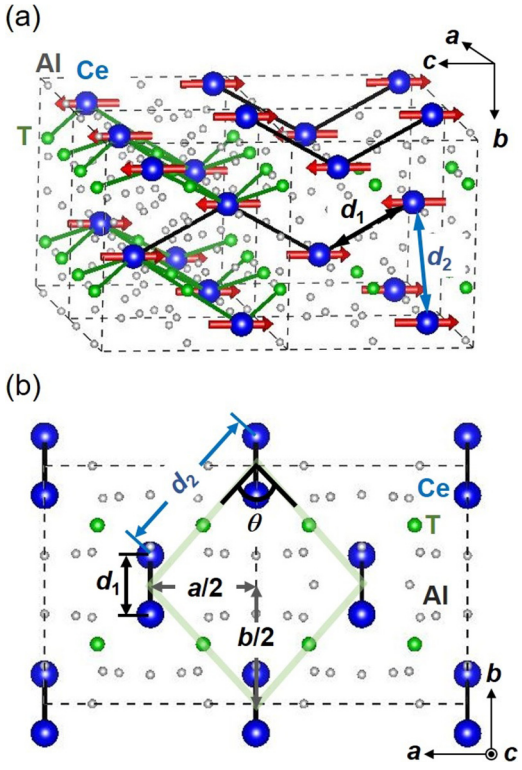

FIG. 1. (a) Crystal structure and antiferromagnetic structure of CeT_2Al_{10} (T = Ru, Os) [10,14]. The first- and second-nearest-neighbor Ce-Ce distances d_1 and d_2 are drawn by arrows. (b) The rhombic arrangement of Ce-Ce chains viewed from the c direction, in which the angle θ is 83 deg for T = Ru and Os at room temperature and ambient pressure.

attributed to the strong c-f hybridization along the a axis [24]. The strong sensitivity of the AFM structure to the pressure and substitution was thought to support the idea that the anisotropic c-f hybridization plays an essential role in the unusual AFM order of CeT_2Al_{10} (T = Ru and Os).

However, the role of anisotropic c-f hybridization has not been fully revealed yet. One of the reasons is that application of hydrostatic pressure uniformly strengthens the c-f hybridization. We recall that application of uniaxial pressure has been more useful to control the ground states of Ce compounds. For example, an AFM order is induced in the nonmagnetic KS CeNiSn when uniaxial pressure is applied along the orthorhombic b or c axis [26]. Thereby, the lattice is elongated perpendicular to the applied pressure; then c-f hybridization along the a axis is weakened. This should promote the localization of the $4f$ electrons, which is in favor of the AFM order.

Motivated by the work on CeNiSn, we have applied uniaxial pressures on CeT_2Al_{10} (T = Ru and Os) to examine the anisotropic responses of the AFM state and c-f hybridization. We report herein the measurements of magnetization and specific heat at low temperatures and strains at room temperature under uniaxial pressures applied along the three principal axes. A part of the results of magnetic susceptibility for T = Os under $P \parallel B$ has been reported in Ref. [27].

II. EXPERIMENTS

Single-crystalline samples of CeT_2Al_{10} (T = Ru, Os) were grown using an Al self-flux method as described previously [8]. Powder x-ray diffraction analysis of the samples confirmed the $YbFe_2Al_{10}$-type structure. The crystals were oriented by the Laue method and shaped by the spark erosion for the measurements of strain, magnetic susceptibility, specific heat, and electrical resistivity, respectively.

The strain was measured by the strain gauge method at room temperature under uniaxial pressures up to 0.25 GPa. Strain gauges were glued on the surfaces of a rectangular sample of $2 \times 2 \times 2\,\mathrm{mm}^3$. The data at pressures above 0.05 GPa were reproducible in the measurements with increasing and decreasing pressures. For the susceptibility measurement, we used a commercial superconducting quantum interference device magnetometer (Quantum Design, MPMS). Uniaxial pressures up to 0.97 GPa were applied on a sample plate of 0.5–0.8 mm in thickness by a homemade pressure cell made of ZrO_2. Two type of pressure cells of 8.8 mm in diameter were used depending on the configurations $P \parallel B$ and $P \perp B$. To observe the spin-flop transition, the magnetization processes $M(B)$ in $B \parallel c$ up to 5 T were measured at 2 K on MPMS. The range of magnetic field for $M(B)$ measurements was extended up to 9.5 T using a high-resolution capacitive magnetometer equipped with a pressure cell [28]. The pressure was determined by measuring the superconducting transition of a piece of tin [29], which was placed at the end of the pressure cell. Under hydrostatic pressures up to 1.24 GPa, the spin-flop field was determined by the measurements of longitudinal magnetoresistance in $B \parallel c$ up to 9.5 T.

The specific heat was measured under uniaxial pressures up to 0.45 GPa by using an ac calorimeter in the temperature range 1.6–40 K [30]. Thereby, we used disk-shaped samples of 2 mm in diameter and 0.2 mm in thickness. The pressure

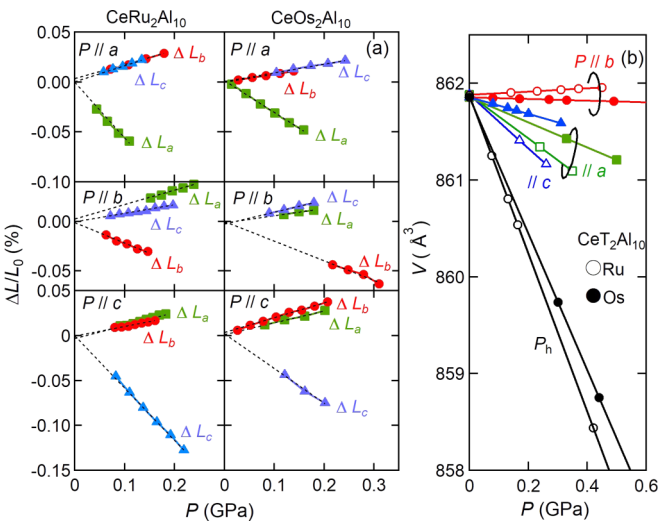

FIG. 2. (a) Variations of the relative change in the length of single crystals of CeT_2Al_{10} (T = Ru, Os) along the three principal axes as a function of uniaxial pressures at room temperature. (b) Variations of unit-cell volume under uniaxial pressures, which are compared with the data under hydrostatic pressure in Ref. [32].

TABLE I. Pressure derivative of the lattice parameters a, b, and c of CeT_2Al_{10} (T = Ru, Os) at room temperature under uniaxial pressures $P \parallel a$, $P \parallel b$, and $P \parallel c$. The data under hydrostatic pressure P_h are taken from Ref. [32].

	P_u (T = Ru)			P_u (T = Os)			P_h (Ref. [32])	
	$P \parallel a$	$P \parallel b$	$P \parallel c$	$P \parallel a$	$P \parallel b$	$P \parallel c$	T = Ru	T = Os
$(1/a_0)da/dP$(%/GPa)	−0.56	0.15	0.15	−0.32	0.07	0.13	−0.32	−0.29
$(1/b_0)db/dP$(%/GPa)	0.14	−0.21	0.11	0.08	−0.20	0.16	−0.28	−0.23
$(1/c_0)dc/dP$(%/GPa)	0.16	0.08	−0.58	0.09	0.12	−0.39	−0.35	−0.30

was determined by the pressure dependence of T_c of a piece of indium [31].

III. RESULTS AND DISCUSSION

A. Variations of lattice parameters

First, we show the uniaxial pressure dependences of the relative length variations $\Delta L/L_0$ for CeT_2Al_{10} (T = Ru, Os) at room temperature in Fig. 2(a). The slope of the data gives the rate $(1/L_0)dL/dP$ (%/GPa), whose values are listed in Table I together with the data measured under hydrostatic pressure, P_h [32]. The lattice parameters perpendicular to the applied pressure increase through the Poison ratio. For T = Ru, the values of contraction rate $(1/L_0)dL/dP$ along the applied pressure for $P \parallel a$ and $P \parallel c$ are similar, whereas that for $P \parallel b$ is 37% of those for $P \parallel a$ and $P \parallel c$. The rates for $P \parallel a$ and $P \parallel c$ decrease by approximately 40% on going from T = Ru to T = Os. The magnitude correlation in $(1/L_0)dL/dP$ under uniaxial pressures is consistent with the smaller value of $(1/b_0)db/dP$ compared with others under hydrostatic pressure [32], as shown in Table I. The weaker response for T = Os than for T = Ru to uniaxial pressures also agrees with that under hydrostatic pressure.

Application of hydrostatic pressure on $CeRu_2Al_{10}$ contracts the lattice in an anisotropic way, where $\Delta b/b_0$ is 80% of $\Delta a/a_0 \simeq \Delta c/c_0$ [32]. The anisotropic contraction is still stronger for the substituted system $Ce(Ru_{1-x}Fe_x)_2Al_{10}$, where $\Delta b/b_0$ is only 50% of $\Delta a/a_0 \simeq \Delta c/c_0$ [33]. This smaller contraction along the b axis in $Ce(Ru_{1-x}Fe_x)_2Al_{10}$ was thought to be the reason for the monotonic decrease in T_N [34]. It contrasts with the appearance of the maximum in T_N under hydrostatic pressure. The different variations of T_N hinted at the strong dependence of T_N on the b-axis parameter.

The set of data of $\Delta L/L_0$ in Fig. 2(a) gives the volume contraction under uniaxial pressures as shown in Fig. 2(b). The volume changes in T = Os under P along the three directions are smaller than in T = Ru. It is noteworthy that the cell volume of both compounds is essentially constant under $P \parallel b$ up to 0.5 GPa.

B. Variations of T_N and $T_{\chi m}$

The temperature dependences of magnetic susceptibility $\chi(T)$ for CeT_2Al_{10} (T = Ru, Os) under uniaxial pressures applied parallel and perpendicular to the external field B are represented in the upper panel of Fig. 3. The data of $\chi(T)$ for $B \parallel a$ and $B \parallel c$ exhibit maxima at $T_{\chi m}$ as indicated by arrows, the temperatures of which are comparable for the two field directions. It should be recalled that the strength of hybridization is related to T_K which is approximated by $3T_{\chi m}$ [2]. Under $P \parallel a$ and $P \parallel c$, $T_{\chi m}$ shifts to high temperatures and the magnitude of $\chi(T_{\chi m})$ decreases in both compounds.

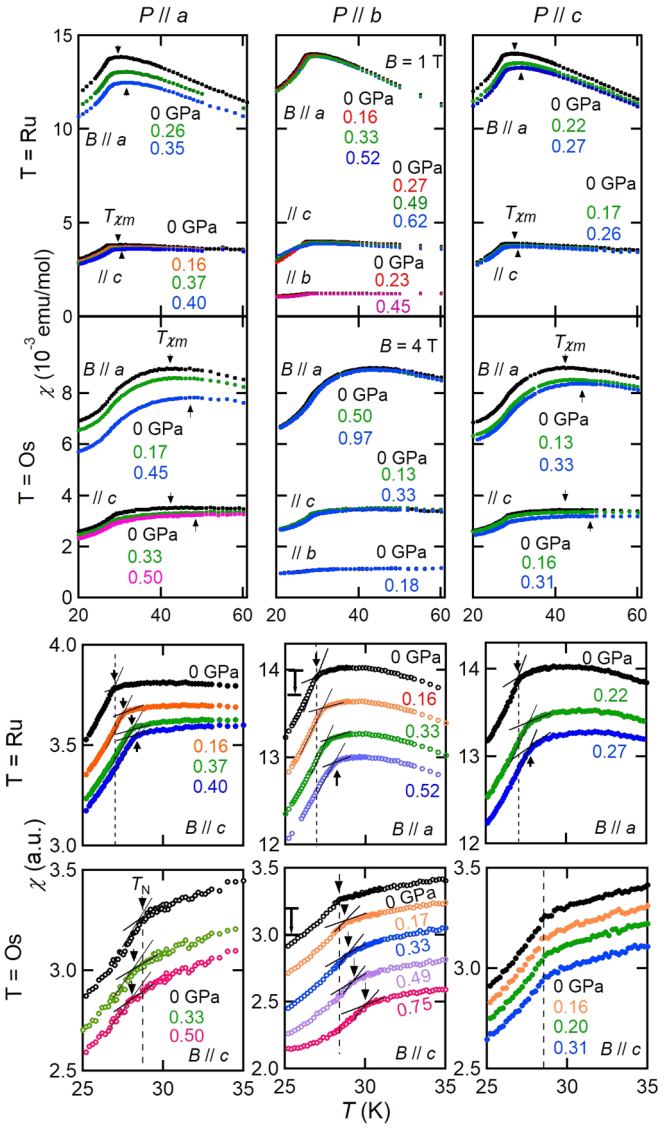

FIG. 3. Temperature dependence of magnetic susceptibility $\chi(T)$ for CeT_2Al_{10} (T = Ru, Os) measured in magnetic fields $B \parallel a$, $B \parallel b$, and $B \parallel c$ under uniaxial pressures $P \parallel a$, $P \parallel b$, and $P \parallel c$. The data near T_N are replotted in the lower panel, where T_N is taken as the intersection of the two lines above and below T_N. For the data only under $P \parallel b$, a suitable offset is added for clarity.

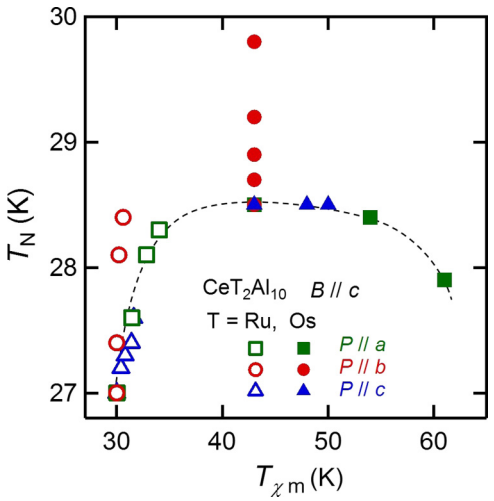

FIG. 4. Variations of T_N for CeT_2Al_{10} (T = Ru, Os) under uniaxial pressures as a function of $T_{\chi m}$, the temperature at the maximum in the magnetic susceptibility $\chi(T)$ for $B \parallel c$.

On the contrary, neither $T_{\chi m}$ nor $\chi(T_{\chi m})$ changes under $P \parallel b$, indicating very weak effect of $P \parallel b$ on the c-f hybridization.

The selected data of $\chi(T)$ in the range 25–35 K are replotted in the lower panel of Fig. 3 to show the variation of T_N. Thereby, the value of T_N was taken as the temperature where the two lines extrapolated from above and below the kink intersect. Upon application of $P \parallel a$ up to 0.5 GPa, T_N for T = Ru increases by 1.5 K, whereas T_N for T = Os decreases by 0.7 K. Under $P \parallel c$, however, the change in T_N for the two compounds is less than 0.1 K. By contrast, application of $P \parallel b$ enhances T_N by 1.2–1.5 K. A similar degree of increase in T_N is observed in the specific heat C divided by temperature (not shown). Using these data, we derived the dependences of T_N on $T_{\chi m}$ and present the results for $B \parallel c$ in Fig. 4. The data of T_N for T = Ru under $P \parallel a$ and $P \parallel c$ are smoothly connected to T_N for T = Os at $P = 0$. Then, T_N for T = Os gradually decreases with increasing $P \parallel a$ and $P \parallel c$. This variation of T_N could be understood by assuming that the c-f hybridization governs the T_N. Under $P \parallel b$, by contrast, T_N of both compounds significantly increases without any change in $T_{\chi m}$. This observation is at variance with the belief that c-f hybridization governs T_N in these KS compounds.

For understanding the unexpected dependence of T_N on $T_{\chi m}$ in Fig. 4, we plot the data of T_N as a function of the lattice parameters in Fig. 5. Thereby, the lattice parameters under pressures were derived from the relative change in the length along the principal axes shown in Fig. 2(a). As a function of the a and c parameters, the variations of T_N under uniaxial pressures are largely different from those under hydrostatic pressure P_h. As a function of the b-axis parameter, however, the data of T_N for T = Ru are linearly increased and smoothly connected with those for T = Os. This relation holds even for both P_h and $P \parallel b$, although the a- and c-axis parameters decrease under P_h but increase under $P \parallel b$. These results of T_N strongly indicate that T_N is enhanced when the b-axis parameter is decreased. It should be noted that the b-axis parameter slightly increases under $P \parallel a$ and $P \parallel c$, as shown in Fig. 2(a). If the T_N is a linear function of the b-axis parameter, then we expect a slight decrease in T_N under $P \parallel a$ and $P \parallel c$. This is confirmed for T = Os, but it is not the case for T = Ru. To understand this discrepancy, it is necessary to examine the possible shift of the atomic coordinate of the Ce atom at the 4c site (0 0.124, 1/4) [17] by x-ray diffraction measurements under uniaxial pressures.

C. Spin-flop transition

As described in Sec. I, the ordered moments μ_{AFM} in the AFM state of $CeRu_2Al_{10}$ are oriented along the c axis, although the a axis is the easy axis in the paramagnetic state. The magnetization $M(B \parallel c)$ exhibits a spin-flop transition from $\mu_{AFM} \parallel c$ to $\mu_{AFM} \parallel b$ when external field is applied along the c axis [23]. We have studied the stability of the unusual AFM state with $\mu_{AFM} \parallel c$ by measuring $M(B \parallel c)$ under uniaxial pressures. As shown in Fig. 6, the spin flop occurs at ambient pressure at $B^* = 5.2$ T, which field agrees with the midpoint of the jump in the magnetoresistance curve shown in the inset of Fig. 6, but is somewhat larger than the reported value of 4.2 T [23]. The magnitude of B^* increases as the uniaxial pressure is applied along the a axis, while B^* does not change

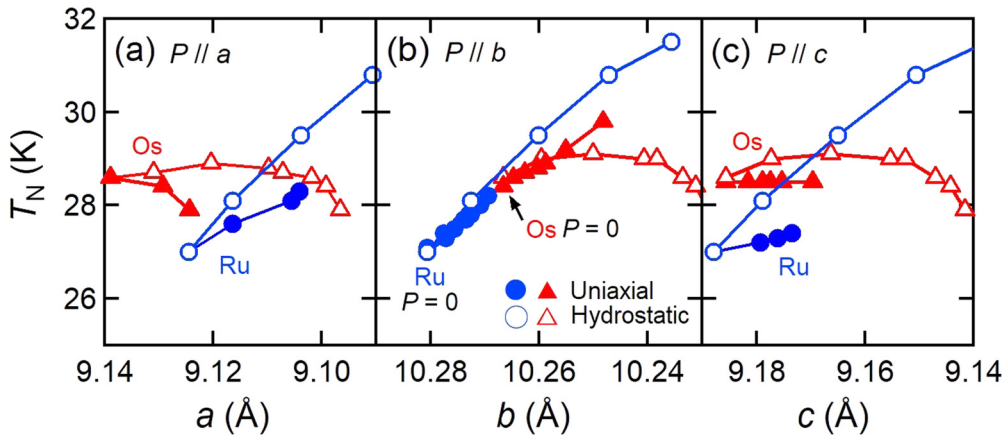

FIG. 5. Variations of T_N for CeT_2Al_{10} (T = Ru, Os) under uniaxial and hydrostatic pressures as a function of the orthorhombic lattice parameters a, b, and c.

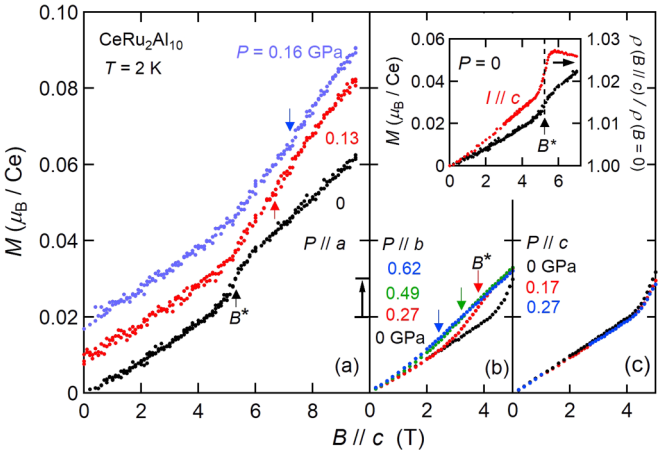

FIG. 6. Isothermal magnetization curves $M(B \parallel c)$ at 2 K for $CeRu_2Al_{10}$ under uniaxial pressures (a) $P \parallel a$, (b) $P \parallel b$, and (c) $P \parallel c$. The data for $P \parallel a$ are offset for clarity. The inset shows the data of $M(B \parallel c)$ and magnetoresistance $\rho(B \parallel c)/\rho(B = 0)$ for the longitudinal configuration at ambient pressure. The magnitudes of the spin-flop field B^* taken as the midpoint of the jump in $M(B \parallel c)$ and $\rho(B \parallel c)$, respectively, agree with each other.

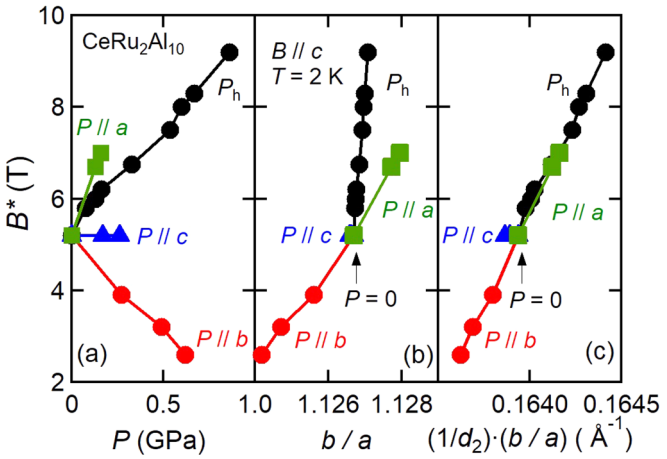

FIG. 7. Spin-flop field B^* for $CeRu_2Al_{10}$ under hydrostatic pressure P_h and uniaxial pressures $P \parallel a$, $P \parallel b$, and $P \parallel c$ as a function of (a) applied pressure, (b) the ratio of lattice parameters b/a, and (c) $(1/d_2)\,(b/a)$, where d_2 is the interchain distance shown in Fig. 1.

for $P \parallel c$. On the contrary, B^* decreases to 2.6 T as $P \parallel b$ is increased to 0.62 GPa. This suppression of B^* under $P \parallel b$ suggests that the difference in the total energy between the two AFM states with $\mu_{AFM} \parallel c$ and $\mu_{AFM} \parallel b$ is diminished by the deformation in the rhombus shown in Fig. 1(b). It is expected that application of $P \parallel b$ increases θ and changes the rhombus to a square. Here, we recall that the AFM state with $\mu_{AFM} \parallel b$ is stabilized even in zero field by the substitution of La for Ce in $Ce_{1-x}La_xRu_2Al_{10}$ at a low concentration $x = 0.1$ [24,25]. As in the case of application of $P \parallel b$, the angle θ is found to be increased by the La substitution. Furthermore, the direction of μ_{AFM} for $x = 0.1$ changes from $\parallel b$ to $\parallel c$ under a weak hydrostatic pressure of 0.3 GPa, while retaining T_N as high as under zero pressure [24,25]. This fact suggests that the mechanism for the high T_N is different from that for orienting μ_{AFM} to the c direction.

The obtained pressure dependences of B^* for $CeRu_2Al_{10}$ are plotted in Fig. 7(a). With applying pressure, $B^*(P_h)$ increases linearly, whereas $B^*(P \parallel a)$ and $B^*(P \parallel b)$ change in opposite directions. The opposite changes suggest that B^* depends on the ratio of lattice parameters b/a. Therefore, these data of B^* are plotted as a function of b/a in Fig. 7(b), where the slope of B^* vs b/a for P_h is much steeper than those for $P \parallel a$ and $P \parallel b$. To describe all the data including that of $B^*(P_h)$, we have searched for an additional structural parameter. As a result, we found that all data of B^* fall on a line as a function of $(1/d_2) \times (b/a)$, as shown in Fig. 7(c). Here, d_2 is the second-nearest-neighbor Ce-Ce distance that is the distance between the zigzag chains as marked in Figs. 1(a) and 1(b). We recall that d_2 decreases under P_h but b/a hardly changes under the condition $\Delta a/a_0 \simeq 1.2\Delta b/b_0$ [32]. When d_2 is decreased, the interchain interaction should be strengthened so that the AFM state with $\mu_{AFM} \parallel c$ is more stabilized. As a result, B^* is increased under P_h. On the other hand, application of $P \parallel b$ should transform the rhombic arrangement of the zigzag chains closer to a regular tetragonal arrangement with increasing θ from 83 deg to close to 90 deg. This transformation may destabilize the AFM state with $\mu_{AFM} \parallel c$, leading to the decrease of B^* under $P \parallel b$. In other words, the antiferromagnetic interchain interaction in the rhombic arrangement realizes the unusual AFM state with $\mu_{AFM} \parallel c$.

IV. SUMMARY

To better understand the mechanism of the unusual AFM order with the high T_N in the KSs CeT_2Al_{10} (T = Ru, Os), we have studied the responses of strain, magnetic susceptibility χ, and specific heat C to uniaxial pressures. First, it is found that application of $P \parallel b$ strongly increases T_N with keeping both the magnitude of $\chi(T)$ and the temperature at the maximum $T_{\chi m}$ unchanged. This finding indicates that the c-f hybridization is not the key parameter determining T_N. Instead, the scaling of T_N by the b-axis parameter for the two compounds confirms the important role of the charge conduction along the b axis in the AFM order. Second, we have analyzed the pressure dependences of the spin-flop transition from $\mu_{AFM} \parallel c$ to $\mu_{AFM} \parallel b$ for $CeRu_2Al_{10}$. The spin-flop field B^* is found to be a linear function of $(1/d_2) \times (b/a)$, where d_2 is the distance between the Ce-Ce zigzag chains. This finding highlights the importance of the interchain interaction in the rhombic arrangement for realizing the unusual AFM state with μ_{AFM} along the c axis.

ACKNOWLEDGMENTS

We acknowledge valuable discussions with S. Kimura, H. Tanida, H. Onimaru, and Y. Kuramoto. We thank D. T. Adroja for critical reading of the manuscript. This paper was partly supported by Japan Society for the Promotion of Science KAKENHI Grants No. JP26400363, No. JP15K05180, No. JP16H01076, and No. JP17K05545.

[1] P. Misra, *Heavy-Fermion Systems* (Elsevier, Amsterdam, 2008).

[2] P. S. Riseborough, Adv. Phys. **49**, 257 (2000) and references therein.

[3] T. Takabatake, F. Teshima, H. Fujii, S. Nishigori, T. Suzuki, T. Fujita, Y. Yamaguchi, J. Sakurai, and D. Jaccard, Phys. Rev. B **41**, 9607 (1990).

[4] M. F. Hundley, P. C. Canfield, J. D. Thompson, Z. Fisk, and J. M. Lawrence, Phys. Rev. B **42**, 6842 (1990).

[5] I. Das and E. V. Sampathkumaran, Phys. Rev. B **46**, 4250 (1992).

[6] A. M. Strydom, Physica B **404**, 2981 (2009).

[7] T. Nishioka, Y. Kawamura, T. Takesawa, R. Kobayashi, H. Kato, M. Matsumura, K. Kodama, K. Matsubayashi, and Y. Uwatoko, J. Phys. Soc. Jpn. **78**, 123705 (2009).

[8] Y. Muro, J. Kajino, K. Umeo, K. Nishimoto, R. Tamura, and T. Takabatake, Phys. Rev. B **81**, 214401 (2010).

[9] D. T. Adroja, Y. Muro, T. Takabatake, M. D. Le, H. C. Walker, K. A. McEwen, and A. T. Boothroyd, Solid State Phenom. **257**, 11 (2017).

[10] D. D. Khalyavin, A. D. Hillier, D. T. Adroja, A. M. Strydom, P. Manuel, L. C. Chapon, P. Peratheepan, K. Knight, P. Deen, C. Ritter, Y. Muro, and T. Takabatake, Phys. Rev. B **82**, 100405(R) (2010).

[11] D. T. Adroja, A. D. Hillier, P. P. Deen, A. M. Strydom, Y. Muro, J. Kajino, W. A. Kockelmann, T. Takabatake, V. K. Anand, J. R. Stewart, and J. Taylor, Phys. Rev. B **82**, 104405 (2010).

[12] G. Morrison, N. Haldolaarachchige, D. P Young, and J. Y Chan, J. Phys.: Condens. Matter **24**, 356002 (2012).

[13] Y. Muro, J. Kajino, T. Onimaru, and T. Takabatake, J. Phys. Soc. Jpn. **80**, SA021 (2011).

[14] S. I. Kimura, T. Iizuka, H. Miyazaki, A. Irizawa, Y. Muro, and T. Takabatake, Phys. Rev. Lett. **106**, 056404 (2011).

[15] F. Strigari, T. Willers, Y. Muro, K. Yutani, T. Takabatake, Z. Hu, Y. Y. Chin, S. Agrestini, H. J. Lin, C. T. Chen, A. Tanaka, M. W. Haverkort, L. H. Tjeng, and A. Severing, Phys. Rev. B **86**, 081105(R) (2012).

[16] F. Strigari, T.Willers, Y. Muro, K. Yutani, T. Takabatake, Z. Hu, S. Agrestini, C.-Y. Kuo, Y. Y. Chin, H. J. Lin, T. W. Pi, C. T. Chen, E. Weschke, E. Schierle, A. Tanaka, M. W. Haverkort, L. H. Tjeng, and A. Severing, Phys. Rev. B **87**, 125119 (2013).

[17] M. Sera, D. Tanaka, H. Tanida, C. Moriyoshi, M. Ogawa, Y. Kuroiwa, T. Nishioka, M. Matsumura, J. Kim, N. Tsuji, and M. Tanaka, J. Phys. Soc. Jpn. **82**, 024603 (2013).

[18] F. Strigari, M. Sunderman, Y. Muro, K. Yutani, T. Takabatake, K.-D. Tsuei, Y. F. Liao, A. Tanaka, P. Thalmeier, M. W. Haverkort, L. H. Tjeng, and A. Severing, J. Electr. Spectr. Related Phenom. **199**, 56 (2015).

[19] J. D. Thompson and J. M. Lawrence, in *Handbook on the Physics and Chemistry of Rare Earths*, edited by K. A. Gschneidner, Jr. *et al.* (North-Holland, Amsterdam, 1994), Vol. 19, p. 383.

[20] H. Tanida, Y. Nonaka, D. Tanaka, M. Sera, T. Nishioka, and M. Matsumura, Phys. Rev. B **86**, 085144 (2012).

[21] K. Umeo, T. Ohsuka, Y. Muro, J. Kajino, and T. Takabatake, J. Phys. Soc. Jpn. **80**, 064709 (2011).

[22] T. Kikuchi, S. Hoshino, N. Shibata, and Y. Kuramoto, J. Phys. Soc. Jpn. **86**, 094602 (2017).

[23] H. Tanida, D. Tanaka, M. Sera, C. Moriyoshi, Y. Kuroiwa, T. Takesaka, T. Nishioka, H. Kato, and M. Matsumura, J. Phys. Soc. Jpn. **79**, 083701 (2010).

[24] H. Tanida, D. Tanaka, Y. Nonaka, S. Kobayashi, M. Sera, T. Nishioka, and M. Matsumura, Phys. Rev. B **88**, 045135 (2013).

[25] D. T. Adroja, A. D. Hillier, C. Ritter, A. Bhattacharyya, A. M. Strydom, P. Peratheepan, M. M. Koza, J. Kawabata, Y. Yamada, Y. Okada, B. Fåk, Y. Muro, T. Takabatake, and J. W. Taylor, Phys. Rev. B **92**, 094425 (2015).

[26] K. Umeo, T. Igaue, H. Chyono, Y. Echizen, T. Takabatake, M. Kosaka, and Y. Uwatoko, Phys. Rev. B **60**, R6957 (1999).

[27] K. Hayashi, K. Umeo, Y. Yamada, J. Kawabata, Y. Muro, and T. Takabatake, J. Phys.: Conf. Ser. **807**, 022002 (2017).

[28] H. Kubo, K. Umeo, K. Katoh, A. Ochiai, and T. Takabatake, J. Phys. Soc. Jpn. **79**, 064715 (2010).

[29] T. F. Smith, C. W. Chu, and M. B. Maple, Cyrogenics **9**, 53 (1969).

[30] K. Umeo, Rev. Sci. Instrum. **87**, 063901 (2016).

[31] J. D. Jennings and C. A. Swenson, Phys. Rev. **112**, 31 (1958).

[32] Y. Kawamura, T. Kawaai, T. Nakayama, J. Hayashi, K. Takeda, C. Sekine, T. Nishioka, and Y. Ohishi, J. Phys. Soc. Jpn. **85**, 044601 (2016).

[33] D. T. Adroja, A. D. Hillier, Y. Muro, J. Kajino, T. Takabatake, P. Peratheepan, A. M. Strydom, P. P. Deen, F. Demmel, J. R. Stewart, J. W. Taylor, R. I. Smith, S. Ramos, and M. A. Adams. Phys. Rev. B **87**, 224415 (2013).

[34] K. Hayashi, Y. Muro, T. Fukuhara, T. Kuwai, J. Kawabara, T. Takabatake, M. Hagihala, and K. Motoya, Phys. Proc. **75**, 121 (2015).